Design Optimization and Control of a Crank-Slider Actuator for a Lower-Limb Prosthesis with Energy Regeneration*

Holly Warner[1], Dan Simon, and Hanz Richter

Abstract— **Recently as technology has progressed, interest in powered prostheses has expanded in an attempt to improve kinematics and kinetics for amputees. The current state of this art is described, noting that most powered knee prosthesis designs do not consider the energy regeneration potential of the natural knee. Three actuator models for the knee joint and its control method are designed, optimized, and evaluated using simulation models. The first model excludes mechanical losses. The second includes a Coulomb friction model. A more coarse efficiency model accounting for the mechanical losses is used in the third case. Energy regeneration of 11.94 J per stride resulted for the first model. The second model gave a total of 7.95 J per stride. Lastly, 1.94 J per stride were regenerated in the third model's simulation. In addition, sufficiently accurate gait tracking was realized with a total RMS error on the order of 10^{-3} rad or less for all models.**

I. INTRODUCTION

Lower limb amputations are frequent among those with diabetes mellitus. In the year 2009 approximately 68,000 hospital discharges in the United States were due to amputations, an increase of 24% over 20 years [1]. In recent years amputations due to traumatic injuries related to military service have increased as well. More than 75% of these were of the lower extremities; 34.5% were transfemoral, indicating loss of both the knee and ankle joints [2].

The majority of above knee amputees currently use passive prostheses such as the commercial Mauch SNS, Rheo Knee, and C-leg. While microcontroller knees, e.g. C-leg, improve upon purely mechanical knees, e.g. Mauch SNS, there are still significant deficits [3]. Both lack knee flexion during stance and ankle plantarflexion during push-off, requirements of proper gait kinematics. This frequently leads to health issues. For example, amputees are 25% more likely than able-bodied individuals to have osteoarthritis [4]. Furthermore, amputees have an 88% probability of osteoporosis. Also, 52% of amputees described chronic back problems [5].

Amputees also expend up to 50% more energy than able-bodied persons [6]. The expense of energy further degrades amputees' quality of life. The source of this loss is primarily prosthetic architectures. Most prostheses use damping and stiffness to regulate the knee and ankle, respectively. Previous research shows that the natural knee has a net negative power (absorption) while the ankle has a net positive power (generation) [7]. Accordingly, passive prostheses incur knee energy losses and cannot provide active ankle push-off.

*This work was supported by National Science Foundation grant 1344954.

The authors are with Cleveland State University, Cleveland, OH, United States.

[1]Corresponding author: h.warner@vikes.csuohio.edu

Recently, the Power Knee has improved mobility by motorizing the knee, but it neglects the ankle [8]. The BiOM active ankle prosthesis is also available but is not made to be integrated with a powered knee [8]. An exception to this dichotomy is a non-commercialized prototype at Vanderbilt University with motors at both knee and ankle [9]. A major drawback to these devices is battery life. The Power Knee usage time is between five and seven hours [10]. The Vanderbilt leg's limit is about two hours of walking [9].

The natural leg likely transfers some excess knee energy to the ankle, a net energy consumer [7]. Powered devices were not designed with this feature of the able-bodied system in mind [11]. Accordingly, it would seem an optimal combination to design an active prosthesis such that gait kinematics and kinetics can be accurately restored, with the capacity for energy regeneration and extended battery life.

The development of a powered and/or energy regenerative prosthesis has been considered in the literature [12], [13], [14], [15], [16], [17]. These designs include electrical, mechanical, and hydraulic approaches. None of these designs power both joints and thus fail to address the proposed need for a fully active, energy regenerative transfemoral prosthesis. Many are limited by the hardware's capacity or efficiency.

Reference [18] proposes that with the recent advent of the supercapacitor an electrically regenerative active knee and ankle prosthesis could be possible. This is inspired by work with hybrid and electric vehicles [19], showing supercapacitors can absorb significant energy in a short period, solving the limitation of [14]. With optimal design of both the mechanical and control systems integrated with a supercapacitor unit, perhaps the efficiency proposed by some of the aforementioned works can be obtained.

The actuator system of such a prosthesis must comply with tight space constraints and generate significant torque as it supports the user's full weight for a time. Alongside these general requirements, the ultimate goals of natural motion and optimal regeneration must be addressed. The crank-slider actuator is commonly used in prosthesis work and could suit these purposes; a proof-of-concept model is given in [18]. Related supercapacitor-based regenerative actuating mechanisms have been studied [20], [21].

In this paper the mechanical and electrical portions of the knee actuator system are developed over several iterations. The applied control is then discussed. This is followed by optimization of the overall actuator. Results are presented, and the paper is concluded with a discussion and some ideas for future work.

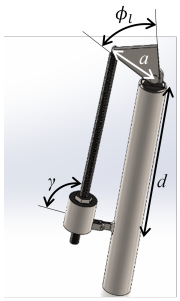

Fig. 1. Notated three-dimensional schematic of crank-slider actuator

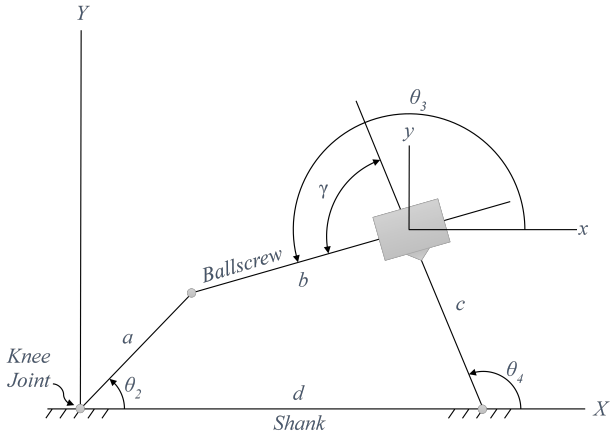

Fig. 2. Geometry definitions used in deriving crank-slider kinematics

II. Actuator Modeling

A representative dynamic model of the system is essential for optimization. Because the primary interest of this work is energy regeneration, bond graph modeling is used [22]. Bond graph modeling is based on power flow, and power is easily integrated to obtain energy. Furthermore, the desired result, the charging of a supercapacitor, involves a multi-domain approach; bond graphs provide a straightforward means of combining the mechanical and electrical systems.

In this section after describing the kinematics, the bond graph modeling method is applied to the prosthesis actuator in several forms. A basic model from previous work [18] is summarized. Two extensions incorporating mechanical losses follow. The first involves creating a complex friction model to observe the effects of mechanical losses on the energy regeneration capacity. A generalized friction model is developed for the second extension.

A. Actuator Kinematics

Fig. 1 depicts a schematic of a prosthetic knee driven by a crank-slider actuator as considered within this paper. A more general form based on [23] was used for kinematic analysis, Fig. 2. Of primary interest is the relationship between the angle θ_2 and b, the variable link length.

$$\theta_2 = \pi + \cos^{-1}\left(\frac{-a^2 + b^2 + 2bc\cos\gamma + c^2 - d^2}{2ad}\right) \quad (1)$$

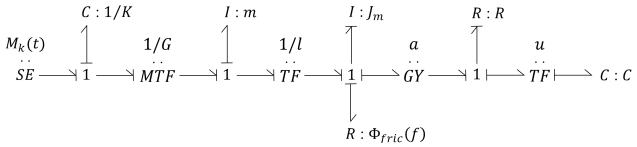

Fig. 3. Bond graph representing the complex friction actuator system. Elimination of the lower R element provides the bond graph for the basic actuator and generalized friction actuator models

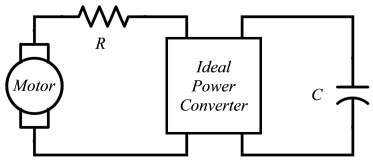

Fig. 4. Circuit representing motor and electronics

One can note from Fig. 1 that there is a further transformation required between θ_2 and ϕ_k

$$\theta_2 = \pi - \phi_l - \phi_k \quad (2)$$

where ϕ_k is the knee flexion angle.

B. Basic Actuator Model Dynamics

An example bond graph is provided in Fig. 3; it describes the complex friction model. To represent the other friction models, one can simply remove the lower R element. Therefore, referring to Fig. 3 and eliminating the lower R element, the basic bond graph model is obtained. The other models are given explicitly in [24]. The input SE is a knee torque profile obtained from able-bodied reference data. From left to right, the elements represent a knee joint torsion spring with constant K, crank-slider geometry defined modulus G, ballnut mass m, ballscrew lead l, motor inertia J_m, motor constant α, armature resistance R, an ideal power converter with modulus u, and a capacitor with capacitance C. Fig. 4 specifies the circuit. The converter shown is linear and without dynamics or losses. Also, G is equivalent to

$$\frac{d\theta_2}{db} = \frac{b + c\cos\gamma}{ad\sqrt{1 - \dfrac{\left(-a^2 + b^2 + 2bc\cos\gamma + c^2 - d^2\right)^2}{4a^2d^2}}}. \quad (3)$$

According to bond graph theory, the causality assignment resulted in the state variables knee velocity, motor momentum, and capacitor current. A through power convention was also established. Consequently, all elements will indicate power exiting the system when the power is positive except SE, which is drawn in the opposite sense. Following the bond graph framework, the system equations can be derived in a straightforward manner. The final result is given as

$$\dot{\phi}_k = Gl\dot{\theta}_m \quad (4)$$

$$\ddot{\theta}_m = \frac{1}{J_m + ml^2}\left(lGM_k - lGK\phi_k - \frac{\alpha^2}{R}\dot{\theta}_m + \frac{\alpha u}{RC}q_C\right) \quad (5)$$

$$i_C = \frac{\alpha u}{R}\dot{\theta}_m - \frac{u^2}{RC}q_C. \quad (6)$$

where ϕ_k is the knee angle, θ_m is the motor angle, q_C is the capacitor charge, and i_C is the capacitor current. A detailed derivation is provided in [24].

C. Complex Friction Actuator Model Dynamics

In the basic actuator case the ballscrew is modeled only by its screw lead as this reflects both the kinematic and kinetic features. This is only one parameter defining a ballscrew; the others—for example diameter, length, and preload—have been left to be determined during future mechanical design. Accordingly, the ability to model mechanical friction is limited because few details of the screw are known; however, to accurately consider the actuator's potential for energy regeneration, the mechanical losses must be estimated.

To address this challenge, a test case could be evaluated. An optimal parameter set, including ballscrew lead, can be determined with the frictionless basic actuator model. A ballscrew with this lead could then be selected based on manufacturers' guidelines and a complex friction model developed from the screw's now known parameters. Simulating this model with these parameters would provide insight into the effect of friction on the system's energy usage.

Ballscrew friction modeling has been a topic of much study ranging from highly complex to simple efficiency models [25], [26], [27], [28], [29]. Selecting among these options is dependent on the accuracy required and available information. For this work the method of [28] was selected.

The addition of a complex friction model requires that a mechanical R element be integrated into the actuator bond graph; this model is Fig. 3. According to [28], the friction of a ballscrew is greatly dependent on the preload of the ballnut and primarily of the Coulomb type.

$$\Phi_{fric}(f) = |\tau_{fric}| \operatorname{sign}(f) \tag{7}$$

Φ_{fric} is a function only of the incoming flow, angular velocity, because of the sign function. Due to the friction being primarily associated with the preload and of the Coulomb form, the friction torque could be represented by the equation typically describing the torque to raise or lower a load with the force F_P set equal to the preload rather than axial load.

$$\tau_{fric} = F_P R_{pitch} \left(\frac{2\pi R_{pitch}\mu \pm l\cos\alpha}{2\pi R_{pitch}\cos\alpha \mp \mu l} \right) \tag{8}$$

In addition to the preload, the pitch radius R_{pitch}, friction coefficient μ, screw lead l, and thread angle α must be known. For a high-precision, lightly preloaded case a value of $\mu = 0.005$ can be used. Additionally, α for a ballscrew is 45^o [28]. The remaining parameters depend on the geometry of the specific ballscrew. R_{pitch} is taken as the ball circle radius [30]. The first set of signs in (8) is for screw extension.

Again deriving the system equations in an algorithmic manner, the final system describing the expanded model can be determined [24]; only the second state equation changes.

$$\ddot{\theta}_m = \frac{1}{J_m + ml^2}\left(lGM_k - lGK\phi_k - \frac{\alpha^2}{R}\dot{\theta}_m + \frac{\alpha u}{RC}q_C - \Phi_{fric}\left(\dot{\theta}_m\right) \right) \tag{9}$$

D. Generalized Friction Actuator Model Dynamics

Alternatively, and perhaps more commonly, ballscrew friction losses are modeled by the screw's efficiency, about 90% [29]. Reference [25] has shown close agreement with this value for various speeds and contact loads, indicating this method's sufficient accuracy for optimization purposes. The complex friction model results should also provide confirmation. The independence of this approach from all screw parameters but l makes it feasible for optimization.

Applying this concept to the model of Fig. 3 with the lower R element eliminated results in a loss of the ideal transformer's power conservation property. This is illustrated in general terms for the case where the screw is converting rotation to translation by

$$F_{screw}\dot{x} = \eta\tau_{screw}\dot{\theta}, \quad \eta < 1. \tag{10}$$

The equations describing a ballscrew are separated into the kinematic and kinetic relationships. Since friction torque is kinetic, it follows that the η should be applied as follows

$$\tau_{screw} = \eta l F_{screw}. \tag{11}$$

It is possible for the screw to be driven by force (backdriving) or torque. For the power equality to hold for both cases and the equations to be of the form (11) as implemented in the bond graph, the coefficient η cannot simply be set to 0.9. The solution to this is to use the equation of the form (11), where η is switched between two values. The first is $\eta_F = 0.9$ for the case where the force is driving the screw. The second is $\eta_\tau = \frac{1}{0.9}$ when the torque is driving the screw.

Replacing the associated fully efficient form in the bond graph system equation derivation process with the form (11) leads to a slight alteration of the second equation of motion of the basic model set of equations derived in [24].

$$\ddot{\theta}_m = \frac{1}{J_m + ml^2\eta}\left(\eta lGM_k - \eta lGK\phi_k - \frac{\alpha^2}{R}\dot{\theta}_m + \frac{\alpha u}{RC}q_C \right) \tag{12}$$

III. Control

Because it would mirror the control of the direct drive system of [18] and provide accurate tracking of reference data, an open-loop controller was selected for testing the regenerative capacity of the system in simulation. The open-loop controller was designed using semi-active modulation for this portion of the work. This system fits the framework for a semi-active system in that the actuator is not directly controlled by an external source; rather, a system variable, u in this case, is modulated to control the flow of power to the actuator from a storage device, namely a supercapacitor.

To determine u, the equations of motion were manipulated such that a direct solution was possible based on reference data. The general case of this method, termed "u-inversion," is established in [31]. The procedure can be outlined for the basic crank-slider actuator model as follows; the others are easily derived in a similar manner [24].

Multiply (6) by q_C.

$$q_C i_C = \frac{\alpha u}{R} q_C \dot{\theta}_m - \frac{u^2}{RC} q_C^2 \tag{13}$$

Perform a change of variables, $q_C = x_3$, $i_C = \dot{x}_3$, and integrate (13) with respect to time.

$$\int_0^t x_3 \dot{x}_3 d\tau = -\frac{1}{RC}\int_0^t (ux_3)^2 \, d\tau + \frac{\alpha}{R}\int_0^t (ux_3)\,\dot{\theta}_m d\tau \quad (14)$$

$$\begin{aligned}\frac{1}{2}\left(x_3(t)^2 - x_3(0)^2\right) = &-\frac{1}{RC}\int_0^t (ux_3)^2 \, d\tau \\ &+\frac{\alpha}{R}\int_0^t (ux_3)\,\dot{\theta}_m d\tau\end{aligned} \quad (15)$$

Solve for $x_3^2(t)$.

$$\begin{aligned}x_3^2(t) = 2\Bigg(&-\frac{1}{RC}\int_0^t (ux_3)^2 \, d\tau \\ &+\frac{\alpha}{R}\int_0^t (ux_3)\,\dot{\theta}_m d\tau\Bigg) + x_3(0)^2\end{aligned} \quad (16)$$

Solve (5) for ux_3, where $x_3 = q_C$.

$$\begin{aligned}ux_3 = \frac{RC}{\alpha}\Bigg(&\left(J_m + ml^2\right)\ddot{\theta}_m - lGM_k(t) \\ &+lGK\phi_k + \frac{\alpha^2}{R}\dot{\theta}_m\Bigg)\end{aligned} \quad (17)$$

Substitution of (17) into (16) gives $x_3^2(t)$ in terms of system parameters and available gait reference data. Taking the square root of this result provides $x_3(t)$. Finally, dividing (17) by this expression for $x_3(t)$ yields a direct solution for u. This method is valid when the capacitor maintains some charge. A negative x_3, for example, interferes with evaluating the square root in addition to being physically impossible. Also, a zero charge would cause the final step to fail.

IV. Optimization

Biogeography-based optimization (BBO) was selected for optimization of the actuator parameters. It is an evolutionary optimization algorithm based on the migration and emigration of species to and from isolated habitats where the habitats represent problem solutions and species characterize solution features [32], [33]. The algorithm tuning parameters include population size, number of generations, number of elite individuals maintained across consecutive generations, and mutation probability; see Table I. The population size was determined such that multiple candidate solutions could meet the constraints (to be described). Observation of the convergence behavior informed the generation limit. The number of elites and mutation rate were based on [18].

As previously indicated, two actuator models were optimized, the basic and generalized friction actuator models. The optimized parameters are shown in Table II, which also includes the search spaces. All of the parameters were allowed to vary throughout a continuous search space except for the ballscrew lead l for which a discrete set was defined.

TABLE I

Biogeography-based optimization parameters used for optimization of the actuator models

Parameter	Value
Population Size	200
Number of Generations	100
Number of Elite Individuals	2
Probability of Mutation per Individual per Generation	0.02

TABLE II

Optimization parameter search spaces for the actuator models

Parameter	Minimum Value	Maximum Value	Units
C	0	500	F
K	0	100	Nm/rad
a	0	0.15	m
d	0	0.3	m
γ	0	π	rad
ϕ_l	0	π	rad
l	1	6.350	mm/rev
q_{C_0}	0	8000	C

This set consisted of the following values in mm/rev: 1, 1.25, 2, 2.5, 3, 4, 5, 5.08, 6, and 6.35. All values greater than and including 2 mm/rev are expected to represent a backdrivable screw [14]. The remaining system variables were fixed values, Table III, selected to coincide with [18].

The minimization cost function was the change in capacitor charge.

$$cost = -(q_{C,final} - q_{C,initial}) \quad (18)$$

Lastly, constraints were enforced to help ensure feasibility. The cost function of any solution violating the constraints was penalized. Specifically, the geometry variables were required to result in real values for the variable length link b (ballscrew) and the transformer ratio G. Additionally, solutions for u resulting from the u-inversion process were required to be real and between -1 and $+1$.

V. Results

A. Basic Actuator Model

An example set of parameters solved by BBO is given in Table IV. Mathematically perfect tracking was attained, indicating that the open loop control method was successful. The total RMS error comparing the simulated knee angle to the reference data is computed as

$$RMS_{total} = \sqrt{\sum_i \left(\phi_{k,i,ref} - \phi_{k,i,sim}\right)^2}, \quad (19)$$

TABLE III

Fixed parameters for all actuator models

Parameter	Symbol	Value	Units
Motor Constant	α	0.054	Nm/A
Armature Resistance	R	0.0821	Ohm
Motor Inertia	J_m	1.29×10^{-4}	kg m^2
Estimated Nut Mass	m	2.1	kg
Link Length	c	0	m

TABLE IV

EXAMPLE SET OF OPTIMIZATION RESULTS FOR THE BASIC ACTUATOR MODEL

Parameter	Symbol	Value	Units
Capacitance	C	221.54	F
Spring Constant	K	47.64	Nm/rad
Link Length	a	0.055	m
Link Length	d	0.25	m
Angle	γ	1.32	rad
Angle	ϕ_l	1.17	rad
Screw Lead	l	5.08	mm/rev
Initial Capacitor Charge	q_{C_0}	6726	C

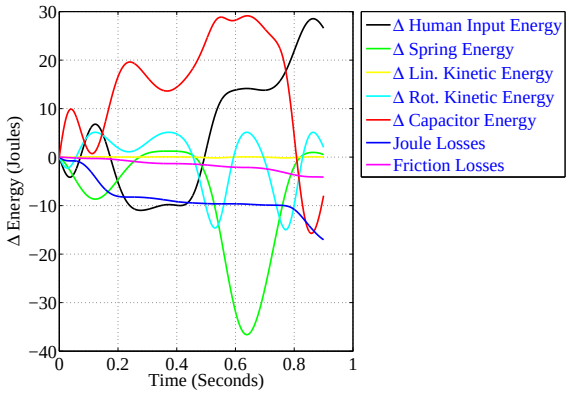

Fig. 5. Plot illustrating the change in energy of each component of the complex friction model. For the given sign convention a negative change in energy corresponds to energy gained by a component

TABLE V

EXAMPLE SET OF OPTIMIZATION RESULTS FOR THE GENERALIZED FRICTION ACTUATOR MODEL

Parameter	Symbol	Value	Units
Capacitance	C	122.89	F
Spring Constant	K	32.32	Nm/rad
Link Length	a	0.061	m
Link Length	d	0.30	m
Angle	γ	0.49	rad
Angle	ϕ_l	1.32	rad
Screw Lead	l	5	mm/rev
Initial Capacitor Charge	q_{C_0}	4078	C

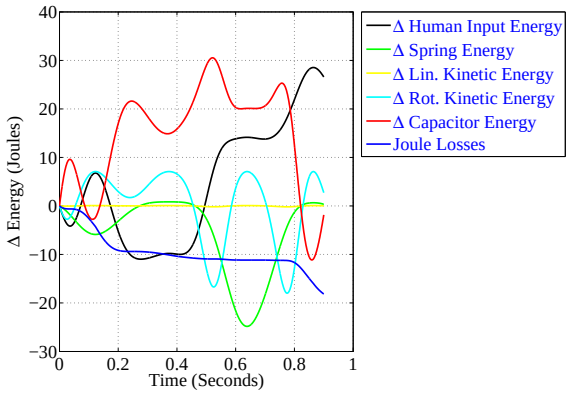

Fig. 6. Plot illustrating the change in energy of each component of the generalized friction model. For the given sign convention a negative change in energy corresponds to energy gained by a component

which resulted in a numerical value of 7.52×10^{-5} rad. For this set of parameters the capacitor charged 0.3932 C during one stride, and the energy increased by 11.94 Joules.

B. Complex Friction Actuator Model

To complete the complex friction actuator model simulation, the optimized parameters of the basic actuator model were coupled with the specific parameters of a ballscrew. The selection of a ballscrew is primarily dependent on the axial load. An equation expressing the axial load of the ballscrew can be derived [24] as implied by the bond graph.

$$F_{axial} = \frac{1}{l}\left(\left(ml^2 + J_m\right)\ddot{\theta}_m + \frac{\alpha^2}{R}\dot{\theta}_m - \frac{\alpha u}{RC}q_C\right) \quad (20)$$

Upon evaluating (20), the peak force was extracted, $F_{axial} = 1421$ N. Coupled with the screw lead 5.08 mm/rev from Table IV, this information was sufficient to select a ballscrew as it also defined the preload value. The optimal preload value is 10% of the maximum force, $F_P = 142.1$ N [28]. A PowerTrac 0631-0200 SRT RA screw and SEL 10408 nut from Nook Industries was selected [34].

Simulation of this model gave $RMS_{total} = 7.9578 \times 10^{-5}$. Over one full stride a gain of 0.2620 C was observed. The change in energy for each component was also evaluated and is shown in Fig. 5. The capacitor gained 7.95 J. The energy entering the system from the human was 26.58 J. The capacitor stored energy represents approximately 30% of this available energy. Looking to future development, the predicted regeneration capacity is equivalent to 26% of the ankle motor requirement according to Winter's data for a fast walking pace [7]. It can also be noted that the losses related to the motor resistance were two to three times greater than the friction losses. Lastly, the lowest ballscrew efficiency reached during a single stride simulation was about 97%, confirming the sufficiency of the manufacturers' value of 90%.

C. Generalized Friction Actuator Model

Example results are provided for one optimization trial with the generalized friction actuator model in Table V. Because the timing of the efficiency switching was determined based on the reference data during the u-inversion process for this case and re-evaluated online during the simulation, the tracking is no longer mathematically perfect. The error of the simulated data versus the reference data was $RMS_{total} = 0.0011$ rad. However, this is still sufficient accuracy for gait.

An alternating pattern between the capacitor and human power flows was observed, representing the power exchange between the human and prosthesis as desired. For this model energy regeneration was successful, though reduced in magnitude as the friction losses totaled 9.67 J. The capacitor had a net increase in charge of 0.056 C. This corresponded to a 1.85 J increase in energy within the capacitor. The change in energy for each component of the actuator system

is depicted in Fig. 6.

VI. Conclusions and Future Work

Three models of a crank-slider actuator and a control method for an active prosthetic leg have been developed and simulated. First, a basic actuator summarizing previous work was presented. The second actuator model explored an approach to modeling a ballscrew's friction based on its geometry and preload. The final method was the implementation of generalized friction losses based on an efficiency percentage, decoupling the ballscrew geometry from the addition of friction to the simulation, allowing greater freedom in optimization because the ballscrew can be modeled simply by its lead as in the basic actuator model.

All three actuator models resulted in an increased capacitor charge over one gait cycle. With each consecutive increase in the total friction, a decrease in the accumulated charge is observed, which is consistent with the models' accuracy.

One future direction for expanding this work is optimizing the motor and perhaps other system features to reduce losses due to the armature resistance. Further considering the energy regeneration capacity, it would be of interest to theoretically determine the maximum limit and compare this value to the optimized results. Additionally, looking toward experimental validation, machine design must be completed. Finally, the models can be extended and evaluated for the ankle joint of a fully actuated prosthesis.

Appendix

The code used to produce the results can be found at `http://embeddedlab.csuohio.edu/Prosthetics/CrankSliderActuator.html`.

References

[1] Centers for Disease Control and Prevention. (2012) Number (in thousands) of hospital discharges for nontraumatic lower extremity amputation with diabetes as a listed diagnosis, United States, 1988-2009. [Online]. Available: http://www.cdc.gov/diabetes/statistics/lea/fig1.htm

[2] C. Krueger, J. Wenke, and J. Ficke, "Ten years at war: Comprehensive analysis of amputation trends," *J. Trauma Acute Care Surg.*, vol. 73, no. 6, pp. S438–S444, December 2012.

[3] B. Hafner *et al.*, "Evaluation of function, performance, and preference as transfemoral amputees transition from mechanical to microprocessor control of the prosthetic knee," *Arch. Phys. Med. Rehab.*, vol. 88, no. 4, pp. 207–217, April 2007.

[4] P. Struyf *et al.*, "The prevalence of osteoarthritis of the intact hip and knee among traumatic leg amputees," *Arch. Phys. Med. Rehab.*, vol. 90, no. 3, pp. 440–446, April 2009.

[5] R. Gailey *et al.*, "Review of secondary physical conditions associated with lower-limb amputation and long-term prosthesis use," *J. Rehabil. Res. Dev.*, vol. 45, no. 1, pp. 15–29, 2008.

[6] A. Gitter, J. Czerniecki, and K. Weaver, "A reassessment of center-of-mass dynamics as a determinate of the metabolic inefficiency of above-knee amputee ambulation," *Am. J. Phys. Med. Rehab.*, vol. 74, no. 5, pp. 332–338, 1995.

[7] D. Winter, "Energy generation and absorption at the ankle and knee during fast, natural, and slow cadences," *Clin. Orthop. Relat. Res.*, no. 175, pp. 147–154, May 1983.

[8] Z. Harvey *et al.*, "Prosthetic advances," *J. Surg. Orthop. Adv.*, vol. 21, no. 1, pp. 58–64, 2012.

[9] F. Sup *et al.*, "Self-contained powered knee and ankle prosthesis: Initial evaluation on a transfemoral amputee," in *Proc. IEEE Int. Conf. Rehabilitation Robotics*, Kyoto, Japan, 2009, pp. 638–644.

[10] Össur. (2010) The new power knee. [Online]. Available: http://assets.ossur.com/lisalib/getfile.aspx?itemid=22240

[11] K. Ingraham *et al.*, "Assessing the relative contributions of active ankle and knee assistance to the walking mechanics of transfemoral amputees using a powered prosthesis," *PLoS ONE*, vol. 11, no. 1, January 2016.

[12] B. Seth, "Energy regeneration and its application to active above-knee prostheses," Ph.D. dissertation, Dept. Mech. Eng., Massachusetts Institute of Technology, Cambridge, MA, 1987.

[13] K. Tabor, "The real-time digital control of a regenerative above-knee prosthesis," M.S. thesis, Dept. Mech. Eng. and Dept. Elect. Eng. and Comp. Sc., Massachusetts Institute of Technology, Cambridge, MA, 1988.

[14] M. Tucker and K. Fite, "Mechanical damping with electrical regeneration for a powered transfemoral prosthesis," in *Proc. IEEE/ASME Int. Conf. Advanced Intelligent Mechatronics*, Montréal, Canada, 2010, pp. 13–18.

[15] J. Geeroms *et al.*, "Ankle-knee prosthesis with powered ankle and energy transfer for CYBERLEGs α-prototype," in *Proc. IEEE Int. Conf. Rehabilitation Robotics*, Seattle, Washington, June 2013, pp. 1–6.

[16] S. Collins and A. Kuo, "Recycling energy to restore impaired ankle function during human walking," *PLoS ONE*, vol. 5, no. 2, p. e9307, February 2010.

[17] A. van den Bogert *et al.*, "Modeling and optimal control of an energy-storing prosthetic knee," *J. Biomech. Eng.*, vol. 134, no. 5, pp. 051 007–1–051 007–8, May 2012.

[18] R. Rarick *et al.*, "Optimal design of a transfemoral prosthesis with energy storage and regeneration," in *Proc. American Control Conf.*, Portland, Oregon, 2014, pp. 4108–4113.

[19] J. Dixon *et al.*, "Electric vehicle using a combination of ultracapacitors and ZEBRA battery," *IEEE Trans. Ind. Electron.*, vol. 57, no. 3, pp. 943–949, March 2010.

[20] H. Richter, "A framework for control of robots with energy regeneration," *J. Dyn. Sys., Meas., Control*, vol. 137, no. 9, pp. 091 004–1–091 004–11, September 2015.

[21] H. Richter, D. Simon, and A. van den Bogert, "Semiactive virtual control method for robots with regenerative energy-storing joints," in *Proc. 19th Int. Federation Automatic Control World Congress*, Cape Town, South Africa, 2014, pp. 10 244–10 250.

[22] D. Karnopp, D. Margolis, and R. Rosenberg, *System Dynamics: Modeling, Simulation, and Control of Mechatronic Systems*, 5th ed. Hoboken, NJ: Wiley, 2012.

[23] R. L. Norton, *Design of Machinery*, 5th ed. New York, NY: McGraw-Hill Education, 2011.

[24] H. Warner, "Optimal design and control of a lower-limb prosthesis with energy regeneration," M.S. thesis, Dept. Mech. Eng., Cleveland State University, Cleveland, Ohio, 2015.

[25] D. Olaru *et al.*, "A new model to estimate friction torque in a ball screw system," in *Product Engineering*, D. Talab and T. Roche, Eds. Springer Netherlands, 2005, pp. 333–346. [Online]. Available: http://dx.doi.org/10.1007/1-4020-2933-0_20

[26] J. Sušeň, "A study on the ball screw friction torque," in *Proc. Student's Conf.*, Prague, Czech Republic, 2011.

[27] A. Kamalzadeh, "Precision control of high speed ball screw drives," Ph.D. Dissertation, Dept. Mech. Eng., University of Waterloo, Waterloo, Ontario, Canada, 2008.

[28] A. Slocum, *Precision Machine Design*. Englewood Cliffs, NJ: Prentice-Hall, 1992.

[29] T. McNier and J. Johnson, *Specifying, Selecting and Applying Linear Ball Screw Drives*, Wood Dale, IL.

[30] H. Huang and B. Ravani, "Contact stress analysis in ball screw mechanism using the tubular medial axis representation of contacting surfaces." *J. Mech. Design*, vol. 119, no. 1, pp. 8–14, March 1997.

[31] H. Richter and D. Selvaraj, "Impedance control with energy regeneration in advanced exercise machines," in *Proc. American Control Conf.*, Chicago, Illinois, 2015.

[32] D. Simon, "Biogeography-based optimization," *IEEE Trans. Evol. Comput.*, vol. 12, no. 6, pp. 702–713, December 2008.

[33] ——, *Evolutionary Optimization Algorithms*. Hoboken, NJ: Wiley, 2013.

[34] Nook Industries. PowerTrac 0631-0200 SRT RA, with SEL ball nut, adjustable preloaded product specification sheet. [Online]. Available: http://www.nookindustries.com/Product/ProductSpec/106544